




## Emergent spiral vortex of confined biased active particles

Deping Huang , Yunfei Du, Huijun Jiang , and Zhonghuai Hou \*

*Department of Chemical Physics and Hefei National Laboratory for Physical Sciences at Microscales, iChEM, University of Science and Technology of China, Hefei, Anhui 230026, China*



(Received 15 February 2021; accepted 15 June 2021; published 8 September 2021)

Confinement is known to have profound effects on the collective dynamics of many active systems. Here, we investigate a modeled active system in circular confinement consisting of biased active particles, where the direction of active force deviates a biased angle from the principle orientation of the anisotropic interaction. We find that such particles can spontaneously form a spiral vortex with two concentric and counter-rotating regions near the boundary. The emerged vortex can be measured by the vortex order parameter which shows nonmonotonic dependencies on both the biased angle and the strength of the anisotropic interaction. Our work can provide an understanding of such dynamic behaviors and enable different strategies for designing ordered collective behaviors.

DOI: [10.1103/PhysRevE.104.034606](https://doi.org/10.1103/PhysRevE.104.034606)

### I. INTRODUCTION

The dynamic behaviors of active systems consisting of self-propelled particles have gained extensive research interest in many fields in recent years. Examples of active particles include not only natural living species such as bacteria [1–3] and spermatozoa [4], but also many artificial objects capable of self-propulsion such as synthesized Janus particles [5] and chiral rotors [6,7]. These systems can be driven far from equilibrium by continuously consuming energy supplied internally or externally, and a wealth of fascinating collective behaviors that cannot be achieved in equilibrium counterparts have been reported both experimentally and theoretically, including motility-induced phase separation (MIPS) [8–11], vortex formation [12], active turbulence [13,14], swarming [15–17], and so on.

In many real systems such as bacterial suspensions and epithelial tissues, active species are usually confined by geometric constraints, which are known to have profound effects on the collective dynamics [3,18–24]. An interesting type of collective behavior is the spiral vortex, wherein the particles rotate collectively in a clockwise or counterclockwise manner [25–29]. For example, Wioland *et al.* reported that motile rodlike bacteria in a droplet spontaneously formed a spiral vortex [12,30], in which cells align in inward spiraling patterns accompanied by thin counter-rotating layers at the boundary. They found that, as confirmed by a subsequent theoretical work [30], cell-cell interactions and hydrodynamic interactions (HIs) between cells play important roles in the formation of a vortex. Recent studies showed that other biological systems such as circularly confined microtubule bundles [31–33] and magnetotactic bacteria [34] can self-assemble into more complex dynamic structures contained

in but beyond the vortex. Despite the key role of HIs in biological systems, there are many hydrodynamic irrelevant systems that can also emerge in interesting vortex states [6,16,35–37], indicating that a HI is not always necessary in the mechanism of the vortex. For example, Vitelli *et al.* studied the dynamic behaviors of ensembles of self-spinning dimmers under circularly geometric frustration [36]. They found that the system self-assembled into a triangular lattice at low density, while as the density is increased, the competition between active rotations and interactions leads to interesting edge currents, whose direction is set by the chirality of the active spinning. Very recently, Zhang *et al.* reported an experimental work where a confined self-spinning macro-rotor (radius  $a = 2.5$  cm) formed a similar robust boundary flow [6]. Aside from the active spinner, actually emergent stable vortices have been reported long before by vibrated granular rods in circular confinement [16,35].

For the vortex-forming species mentioned above, a common feature of them is an aspherical shape, shown as a rigid rod or semiflexible polymer. For active systems consisting of spherical particles, the vortex can also be observed in the presence of underlying alignment effects [6,38–44]. For instance, a previous work by Jacob *et al.* reported that confined active particles, interacting with each other by an inelastic collision rule which favors the motion of two collided particles in the same direction [38], can exhibit a range of collective behaviors from the formation of a vortex to ordered migration. Subsequent experimental work by Bricard *et al.* showed that populations of colloidal rollers under a uniform DC electric field self-organized into a macroscopic steadily rotating vortex [40]. Note that the effective interactions between aspherical objects, e.g., bacteria and the granular rod mentioned above, are essentially anisotropic and highly dependent on the orientations of each object. A well-known example is the Gay-Berne potential [45,46] using distance and orientation as variables to depict the interaction between two ellipsoidlike particles. Furthermore, the alignment effect

\*Author to whom correspondence should be addressed: hzhjlj@ustc.edu.cn

between spherical particles makes the particles move along a preferred direction, which actually reflects some anisotropy of the interactions. Thus the emergent spiral vortex might have some underlying connections with the effective anisotropic interaction, although such a phenomenon has distinct explanations in different active systems.

Here, we employ the so-called biased active particle (BAP) model we proposed recently [47–49] to test this idea. The BAP model describes a kind of spherical Janus particle having two surfaces of different chemistry and/or polarity and thus possesses an essential anisotropic interaction [50,51] between each particle, which is motivated by recent experimental works by Granick and co-workers [5]. Each particle is propelled by an active force that deviates a biased angle  $\theta$  from the principle orientation of the anisotropic interaction, which offers a richer design space for dynamic self-assembly and emergent collective behaviors beyond conventional active particles. Previously, we showed that such BAPs exhibit nontrivial collective behaviors such as reentrant MIPS or directional swarming, due to the intricate cooperation between active propulsion and anisotropic interparticle interactions [47–49]. Here, we show that if confined in a circular space, interestingly, the system consisting of BAPs with a strong enough active force can spontaneously form a stable vortex state with two concentric and counter-rotating spiral layers. We introduce an order parameter to characterize the vortex, which shows nonmonotonic dependences on the biased angle and the strength of the anisotropic interaction. These results indicate that a minimal model including an anisotropic interaction between the active particles can indeed result in spiral collective motions in circular confinement, providing a better understanding of such dynamic behaviors and different strategies for realizing ordered collective behaviors.

This paper is organized as follows. In Sec. II, we describe the model and simulation method. Results and discussion are presented in Secs. III and IV, respectively, followed by the conclusion in Sec. V.

## II. SIMULATION METHOD

We consider here a system consisting of  $N$  BAPs with diameter  $\sigma$  moving in a two-dimensional circular confinement space with diameter  $D$  as shown in Fig. 1. Each BAP is of Janus type consisting of two half disks (the face side colored orange and the back side colored green) which defines an orientation denoted by a unit vector  $\mathbf{q}$  (face side), and it is also propelled by an active force  $F_a$  along a direction given by a unit vector  $\mathbf{n}$  which deviates a biased angle  $\theta$  from  $\mathbf{q}$ . The interaction potential between two BAPs contains two terms,  $U(\mathbf{r}_{ij}, \mathbf{q}_i, \mathbf{q}_j) = U_{\text{WCA}}(r_{ij}) + U_{\text{AN}}(\mathbf{r}_{ij}, \mathbf{q}_i, \mathbf{q}_j)$ , where  $\mathbf{r}_{ij} = \mathbf{r}_j - \mathbf{r}_i$  denotes the vector pointing from particle  $i$  to  $j$  with position vectors given by  $\mathbf{r}_i$  and  $\mathbf{r}_j$ , respectively, and  $r_{ij} = |\mathbf{r}_{ij}|$ . The first term of  $U(\mathbf{r}_{ij}, \mathbf{q}_i, \mathbf{q}_j)$ , also responsible for the interaction between BAPs and the wall, is described by a purely repulsive Weeks-Chandler-Andersen (WCA) potential [52],  $U_{\text{WCA}}(r_{ij}) = 4\epsilon[(\sigma/r_{ij})^{12} - (\sigma/r_{ij})^6 + 1/4]$ , for  $r_{ij} < 2^{1/6}\sigma$  and 0 otherwise, where  $\epsilon$  represents the strength of the WCA potential. The second term is the anisotropic interaction

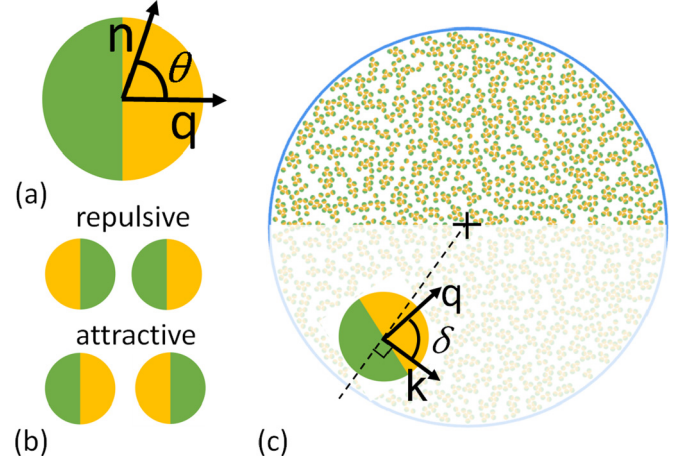


FIG. 1. (a) Schematic diagram of a biased active particle with an angle  $\theta$  between the active direction  $\mathbf{n}$  and anisotropic interaction orientation  $\mathbf{q}$ . The face side is colored orange and the back side green. (b) Configurations of a pair of particles with the strongest repulsive and attractive interactions, respectively. (c) A schematic of the whole system with a circular boundary colored blue. The inset shows an example particle where  $\mathbf{k}$  denotes the tangential vector deviating an angle  $\delta$  from  $\mathbf{q}$ . The black cross denotes the center of confinement.

tion potential given by [53]  $U_{\text{AN}}(\mathbf{r}_{ij}, \mathbf{q}_i, \mathbf{q}_j) = C_J \exp[-(r_{ij} - \sigma)/\lambda](\mathbf{q}_i - \mathbf{q}_j) \cdot \mathbf{r}_{ij}/r_{ij}^2$ , where  $C_J$  is the potential strength and  $\lambda$  denotes the characteristic interaction length. In such a two-dimensional case,  $\mathbf{q}$  is controlled by an angle  $\psi$  and thus  $\mathbf{q} = (\cos \psi, \sin \psi)$ . Accordingly,  $U(\mathbf{r}_{ij}, \mathbf{q}_i, \mathbf{q}_j)$  can be written as  $U(\mathbf{r}_{ij}, \psi_i, \psi_j)$ , where  $\psi_i$  and  $\psi_j$  are the angles of  $\mathbf{q}_i$  and  $\mathbf{q}_j$ , respectively. The anisotropic feature of  $U_{\text{AN}}$  is depicted in Fig. 1(b), where the repulsion between a pair of BAPs is the strongest in the back-to-back configuration, while the attraction is the strongest in the face-to-face configuration. To locate each BAP relative to the circular space, as shown in Fig. 1(c), we also define a tangential vector  $\mathbf{k}$  which deviates an angle  $\delta$  from  $\mathbf{q}$  and is perpendicular to the vector that points from the confinement center to the particle.

The dynamics of BAPs are described by the following overdamped Langevin equations,

$$\dot{\mathbf{r}}_i = \frac{D_t}{k_B T} (-\nabla_{\mathbf{r}_i} \sum_{i \neq j} U(\mathbf{r}_{ij}, \mathbf{q}_i, \mathbf{q}_j) + F_a \mathbf{n}_i) + \sqrt{2D_t} \xi_i, \quad (1)$$

$$\dot{\psi}_i = -\frac{D_r}{k_B T} \nabla_{\psi_i} \sum_{i \neq j} U(\mathbf{r}_{ij}, \mathbf{q}_i, \mathbf{q}_j) + \sqrt{2D_r} \eta_i, \quad (2)$$

where  $\xi_i$  denotes independent Gaussian white noise with zero means and unit variances, i.e.,  $\langle \xi_i(t) \rangle = 0$ ,  $\langle \xi_i(t) \xi_j(t') \rangle = \delta_{ij} \mathbf{I} \delta(t - t')$  with  $\mathbf{I}$  the unit tensor.  $D_t = k_B T / \gamma$  is the translational diffusion constant, where  $\gamma$  is the friction coefficient,  $k_B$  the Boltzmann constant, and  $T$  the temperature.  $D_r$  denotes the rotational diffusion constants, which in the low-Reynolds-number regime is related to  $D_t$  by  $D_r = 3D_t/\sigma^2$ .  $\eta_i$  is also a Gaussian white noise term as  $\xi_i$ . Since the angle  $\theta$  between vectors  $\mathbf{n}$  and  $\mathbf{q}$  is fixed, the second equation determines the evolution of  $\mathbf{n}$  and  $\mathbf{q}$  synchronously.

Reduced units are used in the simulations by using  $\sigma$  and  $\epsilon$  as the basic units of length and energy, and  $\tau = \sigma^2 \gamma / \epsilon$  as the unit of time. In addition, we set  $\lambda = 3.0$ , and  $k_B T = 0.1$ . The

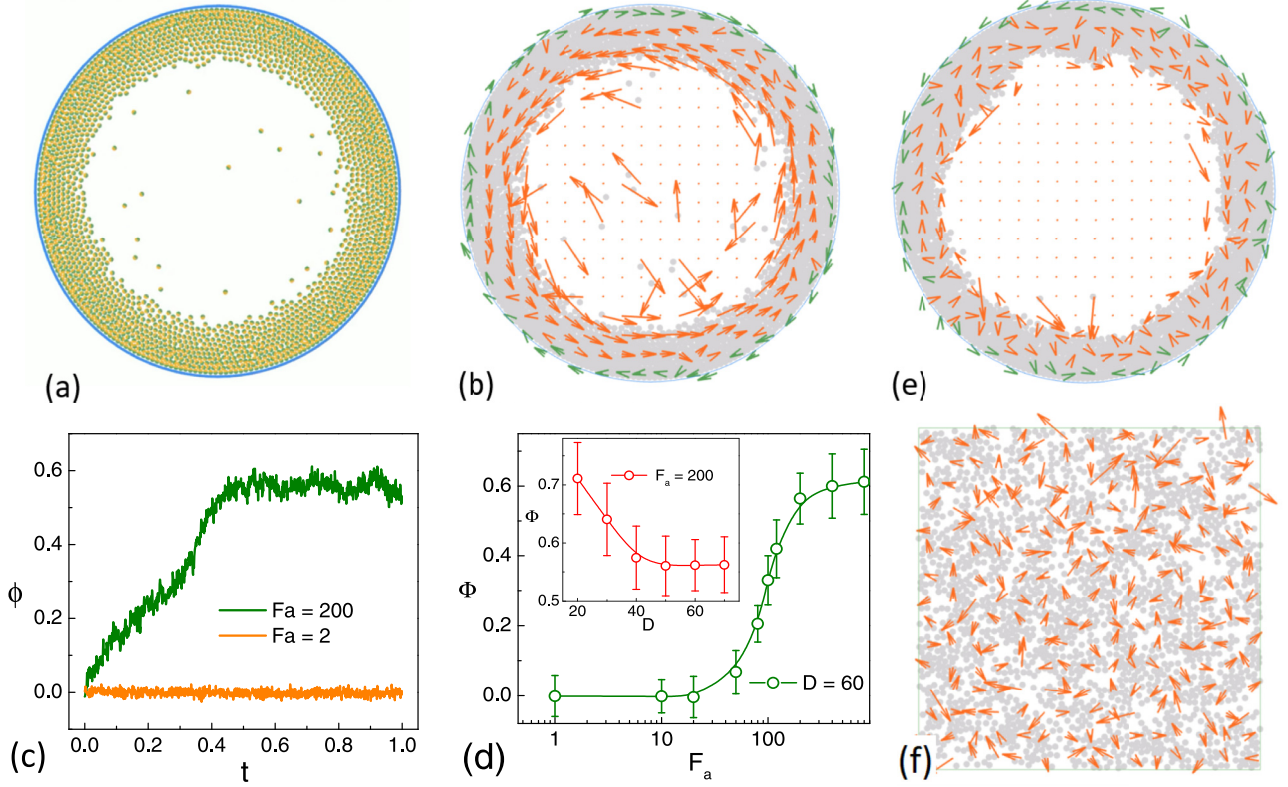


FIG. 2. Emergent spiral vortex. (a) Stable spiral vortex state of a system. (b), (e), (f) Coarse-grained velocity fields, depicted by arrows and obtained by the mean value of velocities in a unit box of size  $3.0\sigma$ , corresponding to confined systems consisting of BAPs and simple ABPs, and an unconfined system consisting of BAPs, respectively. The lengths of the arrows depict the magnitude of velocities, and the arrows in (b) and (e) near the boundary are colored green to distinguish the ones colored red away from the boundary. (c)  $\phi$  as functions of time for systems with  $F_a = 200$  and  $F_a = 2$ . (d)  $\Phi$  as a function of  $F_a$  and the inset shows the relation between the confinement size  $D$  and  $\Phi$ . Lines are drawn to guide the eyes.

system contains 2000 BAPs and the circle diameter is  $D = 60$ , corresponding to an area density  $c \simeq 0.56$ . We start from initial conditions wherein BAPs are randomly distributed inside the whole confined space and the orientations are also randomly chosen from  $(0, 2\pi)$ . A stochastic Euler algorithm is employed to simulate such dynamic equations with a maximal time step  $\Delta t = 10^{-5}\tau$ .

In the present work, we mainly focus on the case for  $F_a = 200$ ,  $\theta = 0.5\pi$ , and  $C_J = 10$  to demonstrate the main observations if not otherwise stated. Note the activity here corresponds to a large value of the Péclet number  $Pe = 2000$  according to the definition  $Pe = F_a\sigma/(k_B T) = \gamma v_p\sigma/(k_B T) = v_p\sigma/D_t$ , where  $v_p$  is the self-propulsion velocity. For a typical colloidal particle with size of a few  $\mu\text{m}$ ,  $v_p$  could reach  $10\text{--}200 \mu\text{m/s}$  [54], while usually  $D_t$  is about  $10^{-2}\text{--}10^{-1} \mu\text{m}^2/\text{s}$ . Therefore,  $Pe$  could vary in a relatively large range. For instance, in Ref. [8], the authors prepared Janus  $\text{SiO}_2$  particles with a radius  $R \simeq 2.13 \mu\text{m}$ , of which the bare diffusion coefficient  $D_0 \simeq 0.029 \mu\text{m}^2/\text{s}$ . At an area fraction  $\phi = 0.27$ ,  $v_p \simeq 1.63 \mu\text{m/s}$ . Therefore, for their system the Péclet number reads  $Pe = 2v_p R/D_0 \simeq 240$ , which is already quite large. Considering the examples shown in the review [54], a Janus particle with size  $20 \mu\text{m}$  can have velocity  $110 \mu\text{m/s}$ , such that  $Pe$  may reach as high as  $100 \times 40/0.02 \approx 20\,000$ , not considering that the bare diffusion coefficient may be smaller than 0.02 (a larger particle

diffuses more slowly). Therefore, the activity occurred in this work can be relevant to experiments.

### III. RESULTS

We start with the investigation on how the dynamic behaviors depend on  $F_a$ . For a relatively small activity, e.g.,  $F_a = 2$  which is closed to a passive case, the system is in a disordered state wherein particles assemble locally to form small clusters and randomly distribute in the whole circular space as shown in Fig. 1(c). Interestingly, if the activity is large enough, a double-spiral-vortex state emerges spontaneously (see Supplemental Material Movie 1 [55]). A typical snapshot of such a state for  $F_a = 200$  is shown in Fig. 2(a), accompanied with a coarse-grained velocity field depicted in Fig. 2(b). One can see that almost all particles accumulate uniformly close to the boundary, and the outermost particles near the boundary rotate clockwise (green arrows) while particles away from the boundary rotate anticlockwise (red arrows).

To quantitatively characterize such a spiral vortex, following Ref. [12], we introduce an order parameter as follows,

$$\phi = \frac{\sum_i |\mathbf{v}_i \cdot \mathbf{k}_i| / \sum_j |\mathbf{v}_j| - 2/\pi}{1 - 2/\pi},$$

where  $\mathbf{v}_i$  is the velocity and  $\mathbf{k}_i$  is the tangential vector of the  $i$ th particle, and  $||\mathbf{v}||$  denotes the norm of  $\mathbf{v}$ . According to



this definition,  $\phi = 1$  for steady azimuthal circulation,  $\phi = 0$  for disordered flow, and  $\phi < 0$  for predominantly radial flow. In Fig. 2(c),  $\phi$  as functions of time for  $F_a = 2$  and 200 are presented. Clearly, for  $F_a = 200$ ,  $\phi$  gradually increases to a steady value of about 0.6 corresponding to a vortex state, while it fluctuates around 0 corresponding to a disordered state for  $F_a = 2$ . To see a global picture, the long-time steady value of  $\phi$  (denoted as  $\Phi$ , averaged over 30 independent runs) as a function of  $F_a$  is drawn in Fig. 2(d). One can see that  $\Phi$  stays at nearly zero for low  $F_a$  and then increases to a plateau for large enough  $F_a$ , suggesting a continual transition from a disordered state to a spiral vortex state. In the inset of Fig. 2(d), the size effect on  $\Phi$  is considered by varying the confinement diameter  $D$  while still maintaining the density of the BAPs. It is shown that  $\Phi$  decreases with  $D$  and finally reaches a plateau for  $D > 50$ , indicating a smaller size of confinement can better facilitate the vortex. For the scope of the present work, to eliminate the size effect, we consider a relatively large confinement as  $D = 60$  in the following.

To highlight the roles of circular confinement and the anisotropic interaction, we have also studied the behaviors for two comparative cases. In the first one, we considered normal active Brownian particles (ABPs) without an anisotropic interaction in the same circular confinement space. As shown in Fig. 2(e), the particles can accumulate near the boundary, which has been known to be a typical feature of ABPs [56–59] when the persistence length  $l_p$  [ $l_p = v_p \tau_p$ , where  $\tau_p = 1/(2D_r)$ ] is larger than the confinement size. Nevertheless, the velocities of the particles are randomly distributed and no spiral vortex can be observed (see Supplemental Material Movie 2 [55]). This demonstrates that anisotropic interactions among BAPs are necessary for the formation of a spiral vortex in the current work. Note  $l_p$  obtained from  $v_p \tau_p$  is not exact for BAPs due to the fact that the activity from self-propulsion is greatly reduced by an anisotropic interaction, and the real value of  $l_p$  for BAPs is hard to estimate in the present scope. Therefore, only when  $v_p \tau_p$  is greatly larger than the diameter of confinement  $D = 60$ , for example, here  $F_a = 200$  corresponding to  $v_p \tau_p \simeq 334$ , can BAPs overcome the attraction from an anisotropic interaction and move to the boundary, forming stable layers. This is the reason that the activity for BAPs must be large. In the second case, we consider BAPs (now with anisotropic interactions) in a periodic box without a confined boundary. As shown in Fig. 2(f), a stable vortex state cannot be observed either, except for some locally fluctuated short-time vortex flows (see Supplemental Material Movie 3 [55]). This indicates that space confinement is also necessary for the formation of a spiral vortex state shown in Fig. 2(b). In short, activity, anisotropic interaction, and space confinement constitute the three key ingredients for the formation of a spiral vortex.

The above observations present an intriguing type of vortex with two concentric and counter-rotating regions near the boundary. To see this more clearly, we cut and zoom into a small piece from the system with a stable vortex, shown in Fig. 3(a). The particles group into distinct layers with different orientations. To locate the position of the different layer, here we just use the radial distribution function  $g(r)$ , defined as  $g(r) = \langle \sum_{i=1}^N \delta[\mathbf{r} - (\mathbf{r}_i - \mathbf{o})] \rangle / \rho^2$ , where  $\rho = N/V$  is the number density and  $\mathbf{o}$  the center of confinement. As

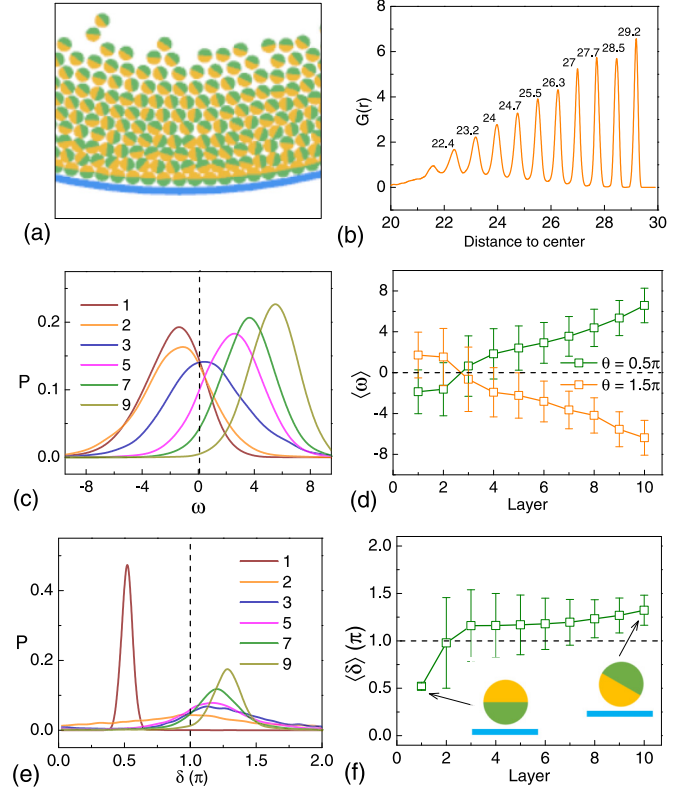


FIG. 3. Characteristics of the spiral vortex. (a) A piece cut from the stable spiral vortex state. (b) Radial distribution function  $g(r)$ . (c), (e) Probability distributions of  $\omega$  and  $\delta$  for a few different layers. (d), (f) Mean values  $\langle \omega \rangle$  and  $\langle \delta \rangle$  as functions of layer identifier. Green and orange dots in (d) correspond to systems with  $\theta = 0.5\pi$  and  $\theta = 1.5\pi$ , respectively. Lines in (d) and (f) are drawn to guide the eyes.

shown in Fig. 3(b),  $g(r)$  has sharp peaks with the variation of  $r$ , marking the average locations of different layers. Then the dynamic behaviors in terms of layers can be readily investigated. Figure 3(c) shows the probability distribution of particle angular velocity  $\omega$  for different layers. The distributions are almost Gaussian, and that for the first two layers (outer layers) peak at negative values, while those for the inner layers peak at apparent positive  $\omega$  values, demonstrating the double-vortex feature where the outer and inner layers rotate in counter directions. Correspondingly, the dependence of the average angular velocity  $\langle \omega \rangle$  on the layer identifier is drawn in Fig. 3(d). As can be seen,  $\langle \omega \rangle$  increases with the layer i.d. from negative to positive values (green curve), identifying the observed rotating structure with thin counter-rotating outer layers. In Fig. 3(d), the same data for a biased angle  $\theta = 1.5\pi$  (orange curve), which is mirror symmetric to the  $\theta = 0.5\pi$ , are also presented. Now a similar double-vortex state can also be observed, except that the rotation directions are reverse compared to those for  $\theta = 0.5\pi$ . In fact, the steady states for biased angle  $\theta$  and  $2\pi - \theta$  are mirror symmetric and we thus only need to consider  $\theta$  with the range  $(0, \pi)$ .

To get more information about the final steady state, we further investigate the distribution of  $\delta$ , the angle between  $\mathbf{q}$  and  $\mathbf{k}$  [Fig. 1(c)], for each layer as presented in Fig. 3(e). Such distributions are also Gaussian-like and peak at two separate

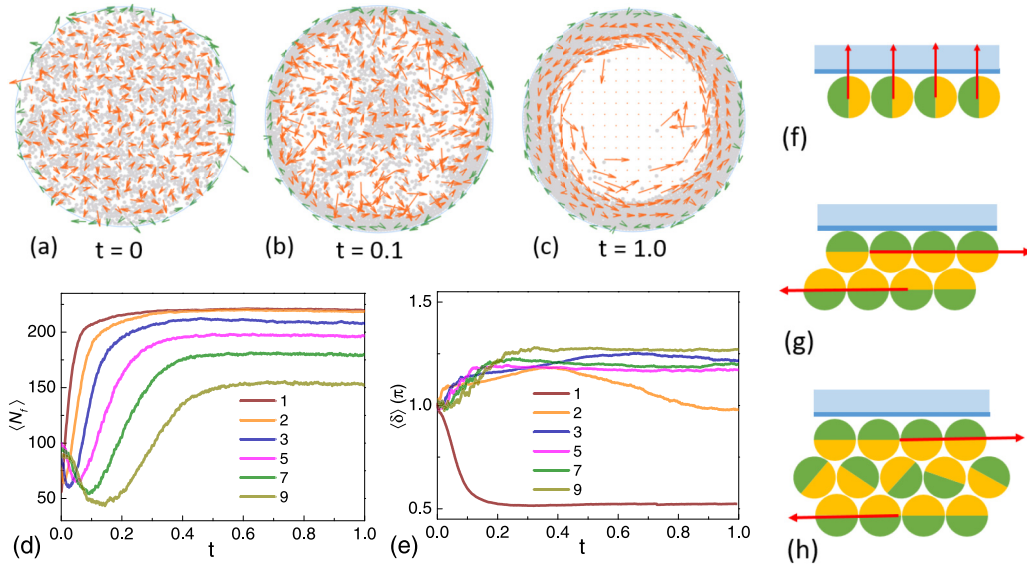


FIG. 4. Mechanism of the spiral vortex formation. (a)–(c) Three typical configurations at  $t = 0, 0.1$ , and  $1.0$ , respectively. The coarse-grained velocity field for layers near and away from the boundary are colored green and red, respectively. (d) Mean numbers of particles ( $\langle N_f \rangle$ ) filled in each layer as functions of time. (e)  $\langle \delta \rangle$  of each layer as functions of time. (f)–(h) Three cartoon pictures show how the vortex emerges. Red arrows depict the orientation of active force.

regimes. Interestingly,  $\delta$  of the first layer distributes quite narrowly around  $0.5\pi$ , while those of all remaining layers distribute more evenly within the range  $(\pi, 1.5\pi)$ . Correspondingly, the mean value  $\langle \delta \rangle$  increases gradually with layer i.d. from  $0.5\pi$  toward  $1.5\pi$  [see Fig. 3(f)]. Since the direction of active force  $\mathbf{n}$  is perpendicular to  $\mathbf{q}$ , there would be net active force along (for  $\delta = 0.5\pi$ ) or opposite (for  $1.0\pi < \delta < 1.5\pi$ )  $\mathbf{k}$  for particles in the outer or inner layers, thus leading to motions along two opposite directions, respectively.

The analyses above indicate that the emergent spiral vortex is actually due to the different arrangement of the particle's orientations which results in net components of active force along the tangential vector. Thus to understand the underlying mechanism of such a vortex state, we need to know why these particles prefer to arrange in this manner. In Figs. 4(a)–4(c), we give typical snapshots of the formation process of a spiral vortex. The system starts from a disordered state with the orientation of coarse-grained velocities chaotically distributed [Fig. 4(a)]. Then parts of the BAPs move toward the boundary and form several initial layers. Meanwhile, the remaining BAPs move to the center, leading to a loose cluster due to the transient motility-induced phase separation, and thus the middle region between the boundary and center becomes dilute [Fig. 4(b)]. One can see that at this time the local velocities of the outer layers have already arranged in a clockwise order as shown by the green arrows, but they are still disordered at other regions (red arrows). Finally, the cluster in the center gradually disappears and the BAPs in it move toward the boundary, forming inner layers which rotate counterclockwise as the red arrows show [Fig. 4(c)]. Therefore these results suggest a two-step process to form a spiral vortex: The outer layers near the boundary rotate first, followed by the inner layers rotating in a counter direction.

To quantitatively describe the transition from the disordered state to the vortex one, we further investigate the mean

number of particles ( $\langle N_f \rangle$ ) and  $\langle \delta \rangle$  of each layer as functions of time shown in Figs. 4(d) and 4(e), respectively. As can be seen,  $\langle N_f \rangle$  of the first and second layer increase quickly and monotonically to a steady value, while  $\langle N_f \rangle$  of the inner layers show nonmonotonic dependences on time which present minima at  $t \simeq 0.1$ , corresponding to the observed dilute region in Fig. 4(b). Meanwhile,  $\langle \delta \rangle$  of the first layer decreases with time from the very beginning and quickly reaches a steady value at  $\pi/2$ , corresponding to the first step mentioned above that the outer layers rotate first, in contrast to the inner layers (e.g., the seventh layer) of which  $\langle \delta \rangle$  still fluctuates around  $\pi$  (namely no net component of active force along the tangential direction). After passing the minimum time,  $\langle N_f \rangle$  of the inner layers increase to steady values and meanwhile  $\langle \delta \rangle$  of such layers increase to a steady value around  $1.2\pi$ , corresponding to the second step that the inner layers rotate in an opposite direction with respect to the outer layers.

Here, we try to give a qualitative explanation for the formation of vortex layers as depicted in Figs. 4(f)–4(h). BAPs first move toward the boundary forming the first layer, with active forces at that time pointing to the boundary, since otherwise BAPs would leave. Owing that  $\mathbf{n}$  is perpendicular to  $\mathbf{q}$  ( $\theta = 0.5\pi$ ), BAPs in such a layer arrange in a face-to-back form [Fig. 4(f)], namely  $\langle \delta \rangle = \pi$ . Then other BAPs move toward the boundary, covering the first layer and forming the second layer. Owing that a face-to-face arrangement is energetically favorable [Fig. 1(b)], BAPs in these two layers would adjust their orientations to minimize the energy cost and thus form a structure with all face sides locating between these two layers [Fig. 4(g)]. Once such a structure is formed, the active force of BAPs in these two layers would align along two opposite directions (both of them are parallel to the tangential direction), respectively. Thus these two layers begin to move collectively, laying the foundation for the emergence of a spiral vortex with two concentric and counter-rotating regions. As more

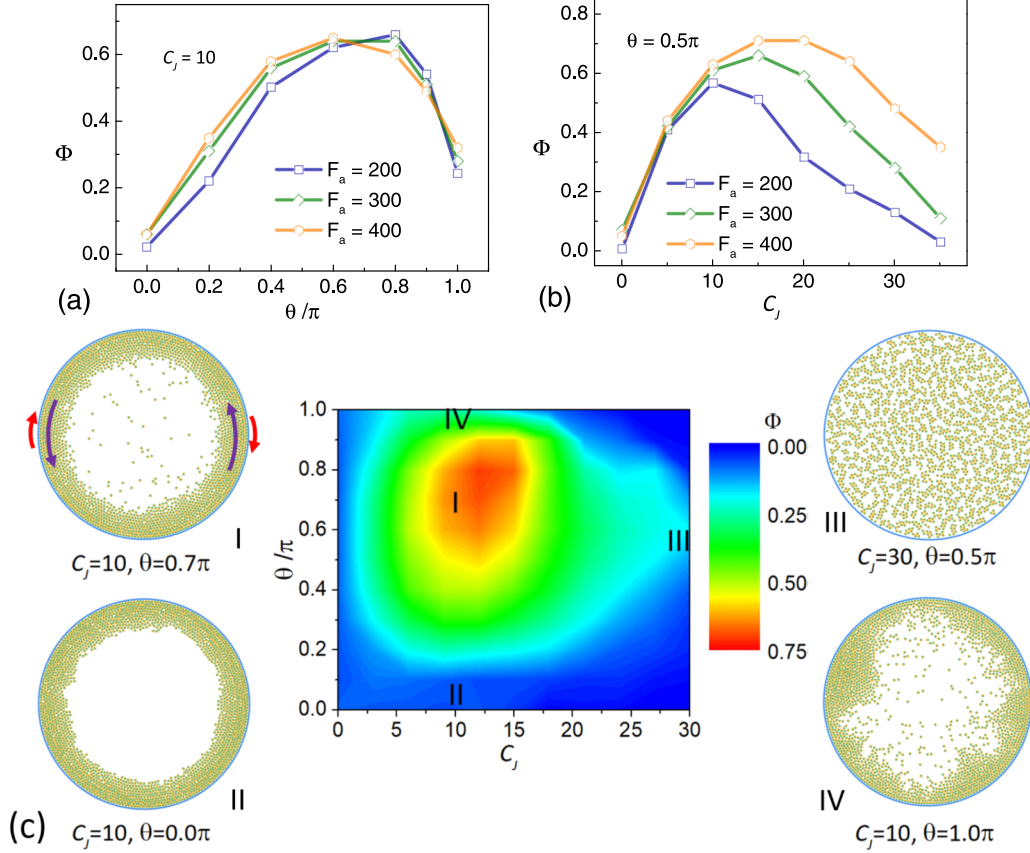


FIG. 5. Global pictures of the vortex formation. (a), (b)  $\Phi$  as functions of  $\theta$  and  $C_J$ , respectively. Three activities are considered, i.e.,  $F_a = 200, 300$ , and  $400$ . (c) Phase diagram of  $\Phi$  in the parameter space of  $(\theta, C_J)$  and the labels I, II, III, and IV locate four points corresponding to four typical configurations shown in (I)–(IV).

BAPs come to form the third layer, their face side can only meet the back side of the second layer to minimize the energy cost. Based on the same reason, the subsequent formed layers also follow the arrangement of the face side of the third layer, and these layers finally swarm collectively to further stabilize the spiral vortex. Also, this is the reason why only thin outer layers rotate clockwise but most of the remaining inner layers rotate counterclockwise. In addition, since the second layer locates at the transition region, the arrangement of the face side would be upset by an effective sheared force and  $\langle \delta \rangle$  of this layer decreases with time in the final stage, indicating a nonmonotonic dependence of  $\langle \delta \rangle$  with time as shown in Fig. 4(e).

In the end, to get a systematic view, we further investigate the effects of the biased angle  $\theta$  and strength  $C_J$  of the anisotropic interaction on the vortex order parameter  $\Phi$  (each value is averaged over 30 independent runs). In Fig. 5(a),  $\Phi$  as functions of  $\theta$  are presented for three activities, i.e.,  $F_a = 200, 300$ , and  $400$ . Interestingly,  $\Phi$  shows clear nonmonotonic dependences on  $\theta$  and achieves the largest values at  $\theta \simeq 0.6\pi$ . For  $\theta = 0$ , the active force acts just along the orientation of the anisotropic interaction, thus BAPs accumulate at the boundary forming static and flattened layers without rotation, as shown in Fig. 5(c)(II). In another limit case where  $\theta = \pi$ , BAPs can also accumulate at the boundary but the structure is highly dynamic and rugged [Fig. 5(c)(IV)], only showing

weak vortex order about  $\Phi \simeq 0.2$ . For  $\theta$  with intermediate values in the range of  $(0, \pi)$ , for instance,  $0.5\pi$ , a stable spiral vortex state emerges as discussed above in detail. According to the schematic snapshots in Fig. 4(h), the face sides of BAPs point to or depart from the boundary in order to minimize the energy cost, thus for  $\theta = 0.5\pi$  where  $\mathbf{n}$  is perpendicular to  $\mathbf{q}$ , the active force would have a maximum component (namely itself) along the tangential direction and would facilitate the collective rotation most. Note that the real optimal value of  $\theta$  locates at nearly  $0.6\pi$  instead of  $0.5\pi$ , which could be a result of the complex interaction between activity and anisotropic interactions in confinement.

Similarly, the dependences of  $\Phi$  and  $C_J$  are shown in Fig. 5(b). As can be seen,  $\Phi$  also presents nonmonotonic dependences on  $C_J$  that it increases to a maximum value and then decreases. When  $C_J$  is set to a very low value corresponding to a negligible anisotropic interaction, BAPs behave more as simple ABPs and thus form static and flattened layers at the boundary as the observed structure of BAPs with  $\theta = 0$  [Fig. 5(c)(II)]. While for another limit case  $C_J$  is very large, BAPs now are more as simple Janus particles and they would quickly assemble into small local clusters from the beginning [Fig. 5(c)(III)], and the active force is powerless to drag the BAPs apart, not to mention the formation of a vortex. Therefore the system can only form a stable spiral vortex for a middle value of  $C_J$ . We also note that the optima



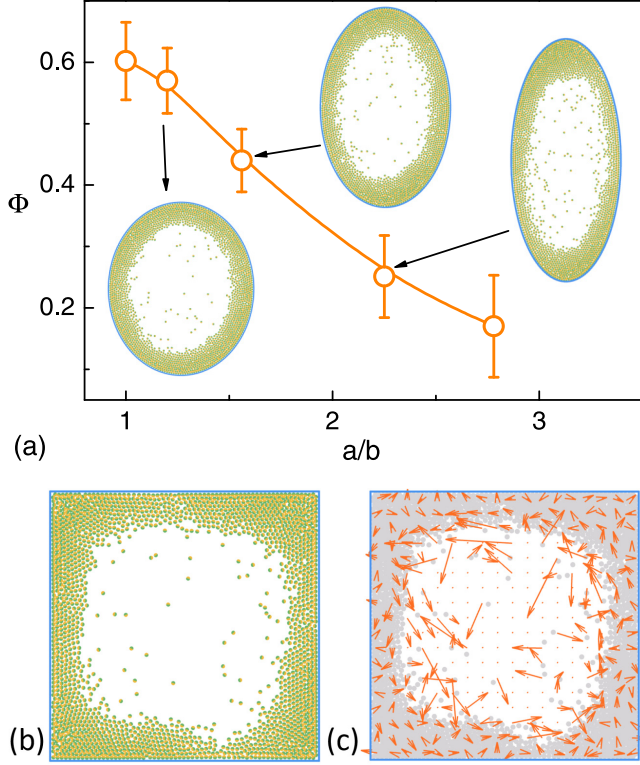


FIG. 6. Shape effects on the vortex. (a)  $\Phi$  as a function of aspect ratio  $a/b$  of an ellipse. Three insets show typical stable configurations of  $a/b = 1.2, 1.5,$  and  $2.25$ , respectively. (b) Stable configuration of BAPs confined in a square box. (c) Coarse-grained velocity field of (b).

of  $\Phi$  increase with  $Pe$  since larger activity can counterbalance the Janus interaction and prevent the formation of small local clusters. Lastly, in Fig. 5(c), we give a phase diagram of  $\Phi$  in the parameter plane spanned by  $\theta$  and  $C_J$ , accompanied by four typical configurations corresponding to four points in such a phase diagram. Clearly, the middle region colored red has the largest value of  $\Phi$ , suggesting that a system with  $(\theta, C_J)$  located in this region would form a stable spiral vortex as shown in Fig. 5(c)(I).

#### IV. DISCUSSION

The confinement in real experiments may always deviate from a perfect circle. Here, we take additional simulations to study the shape effect of confinement on vortex formation. First, we consider an ellipselike shape with a long axis  $a$  and short axis  $b$ , keeping all parameters the same as in Fig. 2(a). The area of the ellipse is fixed, but the aspect ratio  $a/b$  is chosen as a free parameter. As shown in Fig. 6(a), as the confinement space is elongated along the long axis ( $a/b$  increases),  $\Phi$  monotonically decreases. For slight elongation along the long axis, e.g.,  $a/b = 1.2$ , BAPs in such a confined space can still form a stable vortex with also counter-rotating layers near the boundary. However, as the confinement is largely elongated, e.g.,  $a/b = 2.25$ , BAPs would primarily accumulate at the up and down corners as shown in the third inset of Fig. 6(a), leaving a small amount of particles forming

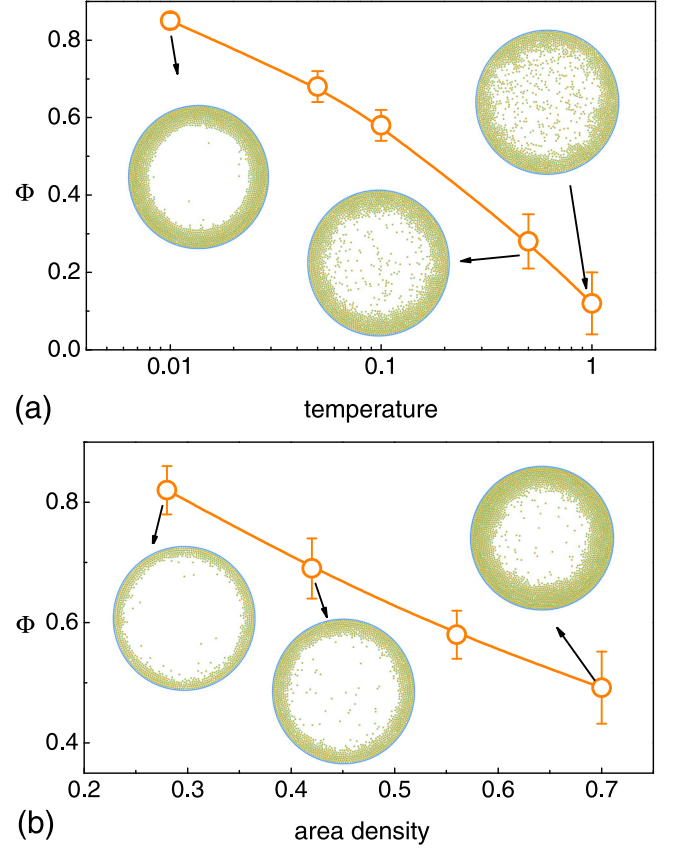


FIG. 7. Temperature effect and density effect on the vortex. (a)  $\Phi$  as a function of dimensionless temperature. (b)  $\Phi$  as a function of area density.

thin layers at the right- and left-hand side. Owing that BAPs at the corner are strongly trapped and can hardly move out, the vortex would be destroyed, as shown by the decrease of  $\Phi$ . Furthermore, we also test the case of square confinement as shown in Fig. 6(b). Clearly, BAPs are also trapped at the four corners and can hardly move collectively. This can be shown by the local velocity field in Fig. 6(c). As can be seen, the directions of local velocities are chaotic and show no apparent vortex order. Therefore, the shape of confinement can greatly influence the formation of a vortex and a perfect circular confinement is most favorable for vortex formation.

In addition, we also discuss the effect of temperature and density on vortex formation. The effects of temperature are shown in Fig. 7(a). With increasing (dimensionless) temperature  $T$  from 0.01 to 1.0, the vortex order parameter  $\Phi$  is greatly decreased from 0.83 to 0.12. The insets show typical snapshots for different temperatures. In general, high  $T$  leads to large fluctuations and destroys the vortex, leading to reduced order. The effects of disk density are shown in Fig. 7(b). One can see that  $\Phi$  also decreases with increasing area density  $c$ . For  $c = 0.28$ , which is a relatively low density, the particles form a few layers near the boundary, but are arranged in a regular manner with stable rotation, while for  $c = 0.7$ , many particles accumulate at the boundary and this results in strong stress to the layers. Such stress compresses the outer particles very closely and meanwhile highly suppresses the motion of these particles.

In the present scope, the hydrodynamic interactions (HIs) between BAPs as well as a BAP and wall are not considered, which may play important roles in the collective behavior of active particle systems as already demonstrated in many articles [12,30–33]. Nevertheless, the very motivation in the present work is to answer such a question: Can such interesting vortex behaviors result from anisotropic interactions among confined active particles? Therefore, we do not consider the HI effect in the current work. Our results demonstrate that HI is not necessary for the formation of vortices if instead an anisotropic interaction exists. As already discussed above, a large Péclet number is required for the formation of double-vortex behaviors. In such a parameter range, we believe that the activity and interactions dominate the behaviors and the HI effect might be weak. However, studying the effect of HI would be an interesting and important topic and it deserves to be a separate future work.

At the end of this section, we would like to discuss briefly about how one may realize a BAP particle in experiments. First, major kinds of active particles are essentially Janus particles. For example, Janus particles with one hemisphere coated with metals may get self-propelled by a chemical concentration gradient, bubbles, laser light, or external fields. Usually, the direction of active force ( $\mathbf{n}$  in the present work) is perpendicular to the coated hemisphere, either to the coated side or opposite to it. On the other hand, Janus particles with one hemisphere hydrophobic and another one hydrophilic can have an anisotropic interaction between each other. Therefore, a Janus particle with one side coated by a metal and the other side with hydrophobic legends could be a candidate for a BAP model, but the angle  $\theta$  is fixed to be 0 or  $\pi$ . Following this idea, to make  $\theta$  tunable, we suggest a possible protocol in which an isotropic particle can be coated by two different layers of materials separately by an aimed biased angle, one of which produces an anisotropic interaction and the other provides self-propulsion.

## V. CONCLUSION

In summary, we have numerically studied the dynamic behaviors of confined biased active particles (BAPs) with an essential anisotropic interaction, where the direction of active force has a biased angle from the principle orientation of the anisotropic interaction. Interestingly, we found that BAPs in circular confinement can spontaneously form a spiral vortex with two concentric and counter-rotating regions near the boundary, while simple active Brownian particles in the same case (with all the same parameters as BAPs instead of the anisotropic interactions) can only form static layers without apparent collective motion. It was revealed that anisotropic interactions, active force, and confinement are the key ingredients for the emergence of a vortex, and particularly the anisotropic interaction induces a different arrangement of BAPs that facilitates collective motion. The emergence of such a vortex can be roughly regarded as a two-step process: Thin layers near the boundary rotate first and then force the other layers away from the boundary to rotate in an opposite direction. We have further studied the effects of biased angle and the interaction strength on vortex formation, finding that moderate values of both are the most favorable. Our work indicates that a minimal model including the anisotropic interaction among active particles can lead to interesting spiral motions in circular confinement, providing an understanding of vortex formation and different strategies for designing smart self-assembled structures.

## ACKNOWLEDGMENTS

This work is supported by MOST (Grants No. 2016YFA0400904 and No. 2018YFA0208702), NSFC (Grants No. 21973085, No. 21833007, No. 21790350, No. 21673212, No. 21521001, and No. 21473165), the Fundamental Research Funds for the Central Universities (WK2340000074), and Anhui Initiative in Quantum Information Technologies (AHY090200).

- 
- [1] J. Dunkel, S. Heidenreich, K. Drescher, H. H. Wensink, M. Bär, and R. E. Goldstein, *Phys. Rev. Lett.* **110**, 228102 (2013).
  - [2] H. P. Zhang, A. Be'er, E.-L. Florin, and H. L. Swinney, *Proc. Natl. Acad. Sci. USA* **107**, 13626 (2010).
  - [3] H. Wioland, F. G. Woodhouse, J. Dunkel, and R. Goldstein, *Nat. Phys.* **12**, 341 (2016).
  - [4] D. Woolley, *Reproduction* **126**, 259 (2003).
  - [5] J. Yan, M. Han, J. Zhang, C. Xu, E. Luijten, and S. Granick, *Nat. Mater.* **15**, 1095 (2016).
  - [6] X. Yang, C. Ren, K. Cheng, and H. P. Zhang, *Phys. Rev. E* **101**, 022603 (2020).
  - [7] F. Kümmel, B. ten Hagen, R. Wittkowski, I. Buttinoni, R. Eichhorn, G. Volpe, H. Löwen, and C. Bechinger, *Phys. Rev. Lett.* **110**, 198302 (2013).
  - [8] I. Buttinoni, J. Bialké, F. Kümmel, H. Löwen, C. Bechinger, and T. Speck, *Phys. Rev. Lett.* **110**, 238301 (2013).
  - [9] P. Dolai, A. Simha, and S. Mishra, *Soft Matter* **14**, 6137 (2018).
  - [10] Z. Ma, Q.-I. Lei, and R. Ni, *Soft Matter* **13**, 8940 (2017).
  - [11] P. Nie, J. Chatteraj, A. Piscitelli, P. Doyle, R. Ni, and M. P. Ciamarra, *Phys. Rev. Research* **2**, 023010 (2020).
  - [12] H. Wioland, F. G. Woodhouse, J. Dunkel, J. O. Kessler, and R. E. Goldstein, *Phys. Rev. Lett.* **110**, 268102 (2013).
  - [13] G. Kokot, S. Das, R. G. Winkler, G. Gompper, I. S. Aranson, and A. Snezhko, *Proc. Natl. Acad. Sci. USA* **114**, 12870 (2017).
  - [14] H. H. Wensink, J. Dunkel, S. Heidenreich, K. Drescher, R. E. Goldstein, H. Löwen, and J. M. Yeomans, *Proc. Natl. Acad. Sci. USA* **109**, 14308 (2012).
  - [15] M. Rubenstein, A. Cornejo, and R. Nagpal, *Science* **345**, 795 (2014).
  - [16] A. Kudrolli, G. Lumay, D. Volfson, and L. S. Tsimring, *Phys. Rev. Lett.* **100**, 058001 (2008).
  - [17] J. A. Cohen and R. Golestanian, *Phys. Rev. Lett.* **112**, 068302 (2014).
  - [18] Y. Du, H. Jiang, and Z. Hou, *J. Chem. Phys.* **149**, 244906 (2018).
  - [19] H. Xu, J. Dauparas, D. Das, E. Lauga, and Y. Wu, *Nat. Commun.* **10**, 1792 (2019).
  - [20] G. Duclos, C. Blanch-Mercader, V. Yashunsky, G. Salbreux, J.-F. Joanny, J. Prost, and P. Silberzan, *Nat. Phys.* **14**, 728 (2018).



- [21] H. Wioland, E. Lushi, and R. E. Goldstein, *New J. Phys.* **18**, 75002 (2016).
- [22] K. Dasbiswas, K. K. Mandadapu, and S. Vaikuntanathan, *Proc. Natl. Acad. Sci. USA* **115**, 201721096 (2018).
- [23] M. Theillard, R. Alonso-Matilla, and D. Saintillan, *Soft Matter* **13**, 363 (2017).
- [24] B. Zhang, B. Hilton, C. Short, A. Souslov, and A. Snezhko, *Phys. Rev. Research* **2**, 043225 (2020).
- [25] S. Rana, M. Samsuzzaman, and A. Saha, *Soft Matter* **15**, 8865 (2019).
- [26] A. C. H. Tsang and E. Kanso, *Phys. Rev. E* **91**, 043008 (2015).
- [27] A. C. H. Tsang and E. Kanso, *Phys. Rev. E* **90**, 021001(R) (2014).
- [28] T. Gao and Z. Li, *Phys. Rev. Lett.* **119**, 108002 (2017).
- [29] I. H. Riedel, K. Kruse, and J. Howard, *Science* **309**, 300 (2005).
- [30] E. Lushi, H. Wioland, and R. E. Goldstein, *Proc. Natl. Acad. Sci. USA* **111**, 9733 (2014).
- [31] K. Suzuki, M. Miyazaki, J. Takagi, T. Itabashi, and S. Ishiwata, *Proc. Natl. Acad. Sci. USA* **114**, 2922 (2017).
- [32] V. Schaller, C. Weber, C. Semmrich, E. Frey, and A. R. Bausch, *Nature (London)* **467**, 73 (2010).
- [33] M. Loose and T. J. Mitchison, *Nat. Cell Biol.* **16**, 38 (2014).
- [34] B. Vincenti, G. Ramos, M. L. Cordero, C. Douarche, R. Soto, and E. Clement, *Nat. Commun.* **10**, 5082 (2019).
- [35] D. L. Blair, T. Neicu, and A. Kudrolli, *Phys. Rev. E* **67**, 031303 (2003).
- [36] B. C. van Zuiden, J. Paulose, W. T. M. Irvine, D. Bartolo, and V. Vitelli, *Proc. Natl. Acad. Sci. USA* **113**, 12919 (2016).
- [37] C. Scholz, M. Engel, and T. Pöschel, *Nat. Commun.* **9**, 931 (2018).
- [38] D. Grossman, I. S. Aranson, and E. B. Jacob, *New J. Phys.* **10**, 23036 (2008).
- [39] A. Bricard, J.-B. Caussin, N. Desreumaux, O. Dauchot, and D. Bartolo, *Nature (London)* **503**, 95 (2013).
- [40] A. Bricard, J.-B. Caussin, D. Das, C. Savoie, V. Chikkadi, K. Shitara, O. Chepizhko, F. Peruani, D. Saintillan, and D. Bartolo, *Nat. Commun.* **6**, 7470 (2015).
- [41] H. Jiang, H. Ding, M. Pu, and Z. Hou, *Soft Matter* **13**, 836 (2017).
- [42] B. Zhang, A. Sokolov, and A. Snezhko, *Nat. Commun.* **11**, 4401 (2020).
- [43] G. E. Pradillo, H. Karani, and P. M. Vlahovska, *Soft Matter* **15**, 6564 (2019).
- [44] P. Liu, H. Zhu, Y. Zeng, G. Du, L. Ning, D. Wang, K. Chen, Y. Lu, N. Zheng, F. Ye, and M. Yang, *Proc. Natl. Acad. Sci. USA* **117**, 11901 (2020).
- [45] W. Chen, Y. Zhu, F. Cui, L. Liu, Z. Sun, J. Chen, and Y. Li, *PLoS ONE* **11**, e0151704 (2016).
- [46] V. N. Kabadi, *Bunsen-Ges. Phys. Chem., Ber.* **90**, 332 (1986).
- [47] Y. Gou, H. Jiang, and Z. Hou, *Soft Matter* **15**, 9104 (2019).
- [48] M. Pu, H. Jiang, and Z. Hou, *Soft Matter* **13**, 4112 (2017).
- [49] Y. Gou, H. Jiang, and Z. Hou, *Chin. J. Chem. Phys.* **33**, 717 (2020).
- [50] Q. Chen, S. C. Bae, and S. Granick, *Nature (London)* **469**, 381 (2011).
- [51] Q. Chen, J. K. Whitmer, S. Jiang, S. C. Bae, E. Luijten, and S. Granick, *Science* **331**, 199 (2011).
- [52] J. D. Weeks, D. Chandler, and H. C. Andersen, *J. Chem. Phys.* **54**, 5237 (1971).
- [53] A. M. Somoza, E. Chacon, L. Mederos, and P. Tarazona, *J. Phys.: Condens. Matter* **7**, 5753 (1995).
- [54] C. Bechinger, R. DiLeonardo, H. Löwen, C. Reichhardt, G. Volpe, and G. Volpe, *Rev. Mod. Phys.* **88**, 045006 (2016).
- [55] See Supplemental Material at <http://link.aps.org/supplemental/10.1103/PhysRevE.104.034606> for the dynamic behaviors of confined and unconfined biased active particles in Movies 1 and 3, respectively, and of confined active Brownian particles in Movie 2.
- [56] X. Yang, M. L. Manning, and M. C. Marchetti, *Soft Matter* **10**, 6477 (2014).
- [57] L. Caprini and U. M. B. Marconi, *Soft Matter* **14**, 9044 (2018).
- [58] J. Tailleur and M. Cates, *Europhys. Lett.* **86**, 60002 (2009).
- [59] S. Das, G. Gompper, and R. G. Winkler, *New J. Phys.* **20**, 15001 (2018).